Interzeolite transformation through cross-nucleation: A molecular mechanism for seed-assisted synthesis

Carlos Chu-Jon,[a] Eli Martinez, [a] Andressa A. Bertolazzo,[a] Suvo Banik, [b,c] Jeffrey D. Rimer ,[d] Subramanian Sankaranarayanan, [b,c] and Valeria Molinero[a]*

[a]Department of Chemistry, The University of Utah, Salt Lake City, Utah 84112-0850; [b]Department of Mechanical and Industrial Engineering, University of Illinois, Chicago, Illinois 60607, United States; [c]Center for Nanoscale Materials, Argonne National Laboratory, Lemont, Illinois 60439, United States; [d]Department of Chemical and Biomolecular Engineering, University of Houston, Houston, Texas 77204

ABSTRACT: Polymorph selection and efficient crystallization are central goals in zeolite synthesis. Crystalline seeds are used for both purposes. While it has been proposed that zeolite seeds induce interzeolite transformation by dissolving into structural units that promote nucleation of the daughter crystal, the seed's structural elements do not always match those of the target zeolite. This discrepancy raises the question of how the seed promotes the daughter phase. Here, we present the first molecularly resolved investigation of seed-assisted zeolite synthesis. Using molecular simulations, we reproduce the fact that a parent zeolite can promote nucleation of a daughter zeolite even when they lack common composite building units (CBUs) or crystal planes. Modeling the seed-assisted synthesis of an AFI-type zeolite using zeolite CHA, our simulations indicate that stand-alone CBUs from the parent seed do not facilitate daughter crystal formation. However, introducing the intact seed significantly reduces synthesis time, supporting that seed integrity is key to increased efficiency. This reduction arises from cross-nucleation of the AFI-type zeolite on the CHA (001) face. We find that parent and daughter zeolites are connected by an interfacial transition layer with order distinct from both zeolites. Simulations reveal that cross-nucleation occurs over a broad range of synthesis conditions. We argue that cross-nucleation would be most favorable for zeolite pairs that share crystalline planes, such as those forming intergrowths. Our findings suggest that the prevalence of intergrowths with a common lattice plane in zeolite synthesis is likely a kinetic effect of accelerated cross-nucleation.

1. INTRODUCTION

Seed-assisted synthesis (SAS) of zeolites involves introducing crystals into the synthesis mixture to facilitate nucleation. The emerging daughter crystals often adopt the same framework as the parent zeolite; however, in some cases, seeding with one crystal (parent) can induce an interzeolite transformation (IZT), resulting in another crystal (daughter) with different structure than the original seed.[1-3] In both scenarios, seeding aids in reducing synthesis time or enabling the selection of a preferred framework.[1, 4-5]

There are two prevailing paradigms about how seeds promote the formation of a different polymorph; both involve the sacrifice of the seed *prior* to the assembly of the target zeolite. The first paradigm assumes that the seed could decrease the nucleation barrier by dissolving, resulting in supersaturations conducive to the daughter crystal's formation.[1, 3] Increase in supersaturation, however, is unlikely to account for polymorph selectivity because it decreases all nucleation barriers and not just that of the target zeolite. It has also been proposed that changes in the Si to Al ratio provided by dissolution of seeds can create conditions that favor the daughter zeolite.[1] This latter mechanism could assist in polymorph selection if the Si/Al ratio of the parent zeolite is closer to that of the daughter, compared to the Si/Al ratio of the reactants in the synthesis.

The second paradigm proposes that some residual "memory" of the seed is maintained after its dissolution. It has been hypothesized that the seed zeolite could dissociate into composite building units (CBUs),[6-7] secondary building units (SBUs),[8-10] silicate rings,[11] or other oligomers[12] that—if they match motifs in the daughter zeolite—would promote its formation. However, the size of oligomers found in solution after the zeolite has formed is small, with typically less than a dozen silicate units, and have structures that do not correspond to those of the SBUs or CBUs of the zeolites synthesized.[13] Moreover, these small oligomers are highly dynamic and reconstruct in times that are short compared to those of zeolite synthesis.[14] The ability of such small dynamic fragments to selectively nucleate zeolites has not been demonstrated.

A seldomly discussed possibility is that the seed can be preserved long enough to lower the nucleation barrier by acting as a substrate for heterogeneous nucleation.[15-16] In this role, the seed could cross-nucleate a different zeolite polymorph. Cross-nucleation has been observed between clathrate

hydrates,[17-18] which are zeolitic water crystals. Within the framework of heterogeneous nucleation theory, cross-nucleation can only occur if the binding free energy of the daughter to the parent crystal is negative, which necessitates a low cost of the parent/daughter interface.[19-20]

Zeolite intergrowths contain stacks of different zeolite frameworks connected through shared crystal planes.[21] The pervasiveness of zeolite/zeolite interfaces in intergrowths indicates that interfaces of zeolites with matching planes have low energetic cost. This suggests that pairs of zeolites that produce an intergrowth could facilitate SAS by cross-nucleation.

Some instances of seed-induced IZT, however, occur with parents and daughters that do not share crystal planes or building units,[4, 22-23] posing the question of what is the mechanism by which the seed promotes the formation of the daughter zeolite. Such is the case of the synthesis of SSZ-24 (AFI) using embryonic SSZ-13 (CHA) seeds.[4] Despite being synthesized with the same organic structure-directing agent (OSDA), N,N,N-trimethyl-1-adamantylammonium ($TMAda^+$), CHA and AFI do not have any common CBUs or planes, and have pores of different connectivity and dimensionality. Nevertheless, CHA seeds robustly promote the formation of AFI under various synthesis condition (see Supporting Information (SI) Section A), resulting in a 7-fold acceleration of zeolite AFI crystallization when all the other conditions of synthesis are equal.[4] Moreover, Tang et al. found experimental conditions in which CHA seeds promote the formation of AFI, while in the absence of CHA a layered silicate is formed[4] (Table S2). These results highlight the role of the seed in polymorph selectivity and enhanced kinetics of the synthesis. The mechanism(s) by which the seed directs the formation of the daughter zeolite are not yet understood.

Experimental methods do not yet have the resolution to unravel the molecular mechanisms involved in interzeolite transformations.[3, 24] *Ab initio* computational methods have been essential in elucidating the geometries, interaction energies, and reaction mechanisms leading to the formation of small oligomers with up to a dozen silica units present during the initial stages of zeolite synthesis.[25-34] However, the expense of *ab initio* methods make them unsuitable to probe the dynamics of nucleation and growth of zeolite crystals. Classical all-atom reactive force fields, such as Reax-FF,[35] which are computationally more efficient than *ab initio* calculations, have been used to study the early stages of zeolite synthesis, reaching the formation of disordered clusters with up to sixty silica units.[36] Currently, only computationally efficient coarse-grained reactive force fields have been able to model the synthesis of zeolite crystals in molecular simulations.[37-44]

To date, these models have been exclusively used to study homogeneous nucleation.[38-39, 43, 45-47] Here, we use a coarse-grained reactive model[43] to investigate whether and how a parent zeolite without a common plane or CBU with a daughter can accelerate the formation of the latter. Coarse-grained simulations are capable of identifying structural aspects such as ring sizes and silica connectivity that lead to zeolite formation. However, it is worth noting that these coarse-grained simulations currently cannot predict the influence of complex OSDA structures, specific pH values, or choice of alkali metals (such as Na^+ and K^+) on zeolite crystallization. As model system, we investigate the homogeneous nucleation of an AFI-like zeolite and the ability of CHA seeds and its CBUs to accelerate its formation.

2. RESULTS AND DISCUSSION

2.1. An AFI-like zeolite nucleates homogeneously in simulations without CHA seeds or CBUs.

To model zeolite synthesis we use an implicit solvent coarse-grained reactive model that represents each silica (SiO_2) unit by a single particle "T" with two- and three-body interactions that promote the Si-Si-Si angles in zeolites[43]. Similarly, the OSDA is modeled as a single particle "S". Here we parameterize S to play the role of $TMAda^+$ used in the synthesis of AFI (see Methods 4.1).

The synthesis of zeolites involves the formation of amorphous precursor phases within which the crystals often emerge.[3, 15] We investigate the nucleation of the zeolite from an amorphous mixture of OSDA and silica in a ratio of 1 to 12 (see Methods 4.2), consistent with the ratio of volumes of silica and OSDA commonly used in the experimental synthesis of AFI.[48]

Zeolites are typically synthesized at temperatures close to 450 K.[15] Even with our highly efficient coarse-grained model, the glassy dynamics of silica at these temperatures make the synthesis too slow for the molecular simulations. To enable faster crystallization, we evolve our simulations at 620 K, approximating the higher temperatures of ultrafast zeolite synthesis.[49]

The nucleation and growth of the zeolite are monitored using an order parameter that discerns between zeolites and amorphous precursors (see Methods 4.3). We collect 49 independent trajectories of crystallization starting from the amorphous mixture in the absence of CHA or its CBUs (Figure S2). A zeolite with one-dimensional pores nucleates homogeneously from the precursor mixture (Figure 1) with an average nucleation time of 164 ns (Table S3). The crystallization is accompanied by a sudden drop in the potential energy that can also be used to monitor the formation of the zeolite. The higher temperatures of the simulations and the lack of explicit Si-O bonds in the coarse-grained model that would require slow hydrolysis and condensation reactions to restructure the silica network make the time scales of the synthesis in the simulations orders of magnitude shorter than in the experiments.[37]

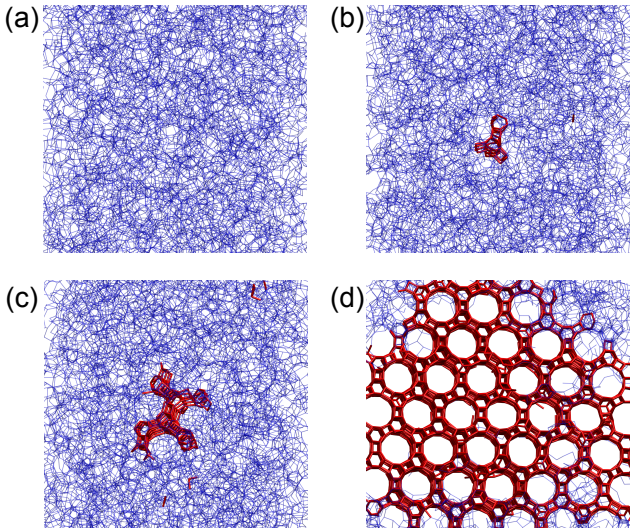

Figure 1. Homogeneous nucleation of AFI' in un-seeded simulations. The zeolite is shown in red and the amorphous phase in blue (OSDAs are omitted for clarity). Snapshots (a)-(d) show the temporal progression of nucleation and growth of AFI' over time during synthesis.

The zeolite that nucleates from the amorphous mixture possesses 1D pores with 12-member rings identical in symmetry and size to those in AFI (SI Section C). There are only minor differences in the orientation of the six-member rings that tile the pores in AFI and the zeolite obtained in the simulations (SI Section C). Hence, we consider the zeolite nucleated in the simulation a suitable proxy of AFI and call it AFI'. We find that AFI' also nucleates homogeneously from a precursor mixture with 1 OSDA for every 8 silica, supporting that the 1D zeolite forms robustly with changes in the reactant ratios (Table S4). This result aligns with the experimental findings by Tang et al., [4] reproduced in Table S1. In what follows, we investigate the ability of CHA and its CBUs to promote the formation of the AFI' zeolite.

2.2. Dispersed CBUs of CHA do not promote the nucleation of AFI'.

It has been hypothesized that CBUs can break off from the seed during its dissolution and participate in the crystallization of the daughter zeolite.[6-7] If that were the case, these CBUs would initially reside in the solution alongside the reactant species. To test whether CBUs released from the CHA seed into the solution could promote the nucleation of the daughter crystal, we perform simulations that start with a single chabazite cage (*cha* CBU) in the simulation cell. The CBU is represented as a rigid body to prevent its dissolution or restructuring. Silica and OSDA are randomly inserted in the cell in the same ratio of 12:1 used for the homogeneous nucleation simulations of Section 2.1 (see Methods 4.2). We find that the monomers preferentially attach on the surface of the *cha* CBU, developing a spherical amorphous particle ~7 nm in diameter after 150 ns of deposition at 620 K (Figure 2). Such size is typical of amorphous precursors of zeolite synthesis (SI Section F).[50-51] We stop the deposition and further evolve the system at 620 K for 390 ns, when AFI' nucleates from the nanoparticle. We find that the nucleation not only takes longer than in the absence of the CBU seed, but also that the AFI' nucleus is not adjacent to the *cha* CBU (Figure 2), indicating that the nucleation is homogeneous.

To verify that the lack of AFI' nucleation by the CBU is not the result a lower stability of the zeolite in the ~7 nm diameter nanoparticle,[45] we evolve 10 simulations in which one *cha* or double-6-membered-ring (*d6r*) rigid CBU is inserted into the same periodic simulation cell of amorphous precursor employed for the homogeneous nucleation simulations in Section 2.1. Same as for the nanoparticle, we find that AFI' nucleates and grows homogeneously in these simulations (Figure 3), with times that are comparable to those of the homogeneous nucleation studies in Section 2.1 (Table S3).

To assess whether the presence of multiple CHA CBUs in the same simulation cell can promote the nucleation of the AFI' zeolite we perform independent nucleation simulations, introducing 8 *d6r*, 10 *d6r*, or 8 *cha*, and a combination of 4 *d6r* and 4 *cha* CBUs into the amorphous precursor mixture used for the homogeneous nucleation (Methods 4.2.). Table S3 shows that even the presence of multiple CBUs does not facilitate the nucleation of AFI' (Figure 3 and SI Movie 1). Considering the similarity of AFI and AFI' and their lack of CBUs in common with CHA, our results suggest that if CHA were to release whole CBUs into the synthesis mixture and these remained intact in solution, they would not promote the formation of AFI.

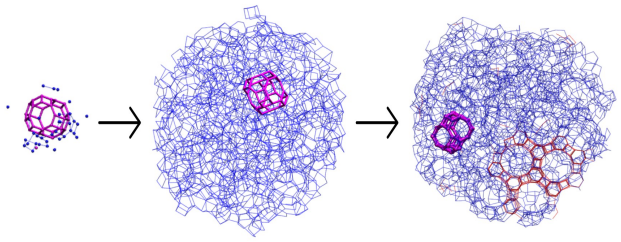

Figure 2. Composite building unit *cha* (magenta) acts as the nucleation site for an amorphous OSDA:silica nanoparticle (blue) from a dilute solution, but does not promote the nucleation of AFI' (red). The early stages show monomers condensing on the CBU (left and center images). After 200 ns, the CBU is encapsulated in a 7 nm amorphous nanoparticle. After the nanoparticle has formed, it takes an additional 390 ns for the (homogeneous) nucleation of AFI (right image). Movie 1 presents the full nanoparticle growth and crystallization process.

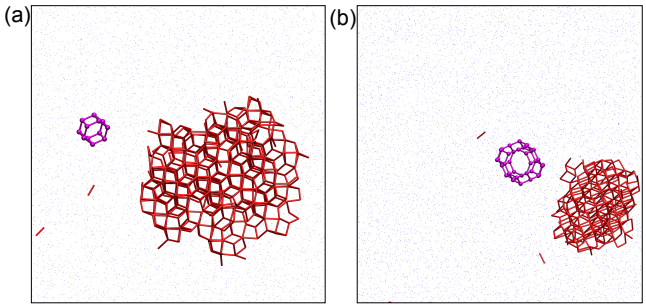

Figure 3. Homogeneous nucleation of AFI' (red) in the presence of (a) *d6r* and (b) *cha* composite building units The CBUs are colored magenta, amorphous T particles are shown with blue dots, and OSDAs are omitted for clarity. The CBUs do not reduce the nucleation time of AFI' (Table S3).

2.3. CHA seed accelerates formation of the target zeolite through cross-nucleation.

To assess the possibility of seed-assisted synthesis through cross-nucleation, we expose pre-equilibrated amorphous mixtures of silica and OSDA with 12:1 or 8:1 silica to OSDA ratios to a rigid crystalline slab of purely siliceous CHA zeolite exposing the (001) plane (Methods 4.2).

We collect 34 independent trajectories of crystallization of the amorphous mixture with the 12:1 silica to OSDA ratio in contact with a CHA slab (i.e., seed). We observe nucleation of AFI' in all sampled trajectories; ninety percent of these simulations nucleate AFI' within the immediacy of the CHA interface (Figure 4). The presence of the CHA seed results in a 24-fold acceleration of AFI' nucleation compared to the homogeneous nucleation from the same synthesis mixture and temperature (SI Section B and Table S3). Moreover, AFI' consistently nucleates at the CHA interface, with its 1D channels perpendicular to the CHA surface (Movies 2 and 3). These results confirm CHA's role not only in promoting AFI' but also in determining its epitaxial orientation (Figure 4 and SI Section D).

The well-defined orientation of AFI' (Figure 4 and SI Section D) and 24-fold decrease in AFI' nucleation times at the CHA interface confirm that CHA heterogeneously nucleates AFI'. The speed-up in the simulations agrees qualitatively with the reported 7-fold reduction in AFI synthesis time when employing CHA seeds compared to non-seeded synthesis and otherwise identical conditions[4] (Table S1). Exact agreement between experiments and simulations is not expected because the ratio of heterogeneous to homogeneous nucleation times decreases with reduced temperature (SI Section B) and also depends on the amount of seeds;[4] however, in both the simulations and the experiments under a large range of conditions[4] (Table S2), the presence of the CHA seed accelerates the crystallization of the daughter zeolite.

Tang et al. [4] showed that the CHA seed's promotion of AFI is consistent against variations in the silica to OSDA ratio (SI Section A). Likewise, we find that simulations of synthesis with 1:12 and 1:8 OSDA-to-silica ratio heterogeneously nucleate AFI' at the CHA (001) interface (Tables S3 and S4). We conclude that the promoting effect of CHA on the synthesis of the daughter zeolite is robust to changes in the ratio of silica to OSDA in both the experiments[4] and simulations.

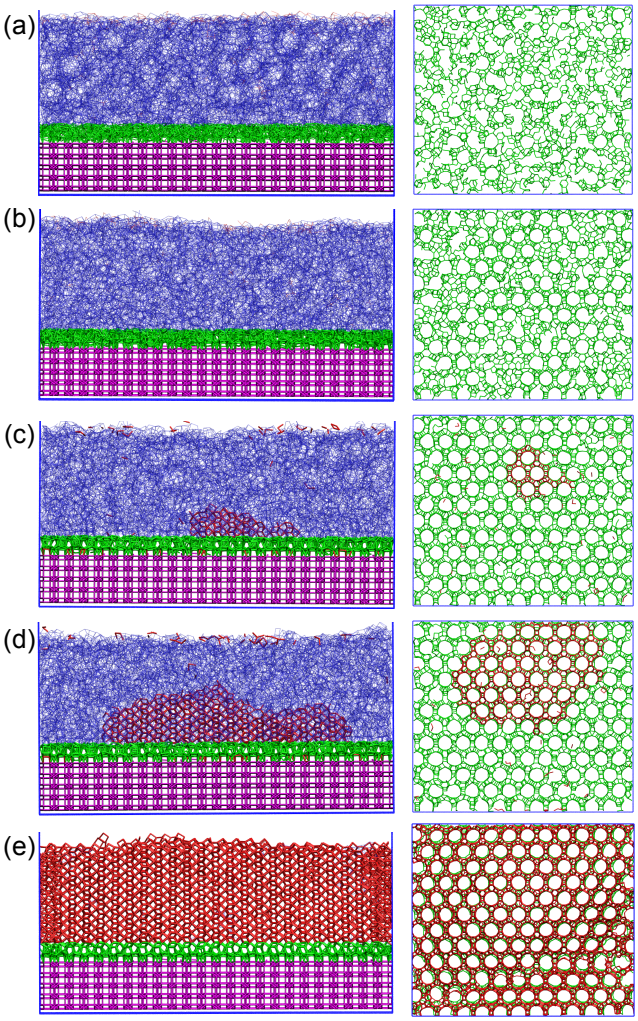

Figure 4. Cross-nucleation of zeolite AFI' on the (001) face of zeolite CHA. Snapshots (a) to (e) show progressing times along the nucleation and growth of AFI' along the synthesis (see also Figure S6, Movie 2, and Movie 3). The silica framework of CHA is shown in magenta, the one of AFI' in red, the amorphous mixture in blue, and the interfacial transition layer between CHA and AFI' is shown in green. OSDAs are not shown. The left and right panels display side and top views of the simulation cell. For clarity, only the interfacial layer and the AFI' zeolite are shown in the right panels.

2.4. An ordered interfacial transition layer connects AFI' to CHA.

CHA does not have any crystal planes in common with AFI, making their interface not readily apparent. We find that CHA and AFI' connect through a ~6 Å-wide ordered interfacial transition layer (ITL) that bridges the distinct silica connectivity in the two zeolites (Figure 5 and SI Section E). The simulations reveal that the ITL forms at the CHA/amorphous interface prior to AFI' crystallization and subsequently facilitates the nucleation of the daughter crystal (Figure 4a-c and SI Section E). This sequence of events supports a consecutive, two-stage process of cross-nucleation.

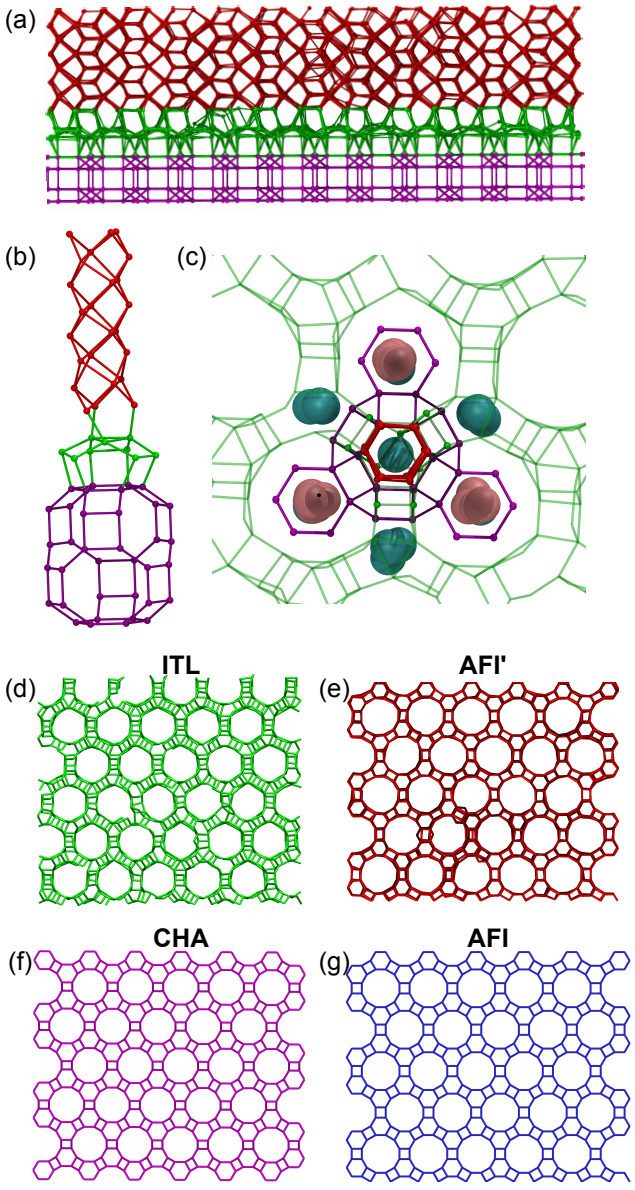

Figure 5. Silica order at the CHA/AFI' interface and order in congruent zeolite planes. (a) Side view of a CHA slab (purple), and the ITL (green) and AFI' (red) formed during the synthesis. (b) Detail of the interface, depicting the connectivity between the *cha* cage of CHA (purple), the distinct 9-sided cage of the ITL (green), and the pore wall of AFI' (red). (c) Top view of the interface showing the position of the OSDAs residing below the ITL (teal balls) and at or above it (pink balls); backbone color code as in panels (a) and (b). (d) Top view of the ITL; (e) AFI' plane parallel to the interface (perpendicular to the 12-member ring channels), (f) a single CHA layer parallel to the interface , and (g) plane of AFI in the direction perpendicular to the 12-member ring channels.

Tang et al. credited CHA's capacity to expedite AFI crystallization to the abundance of 6-member rings in both CHA and AFI.[4] While our analysis indicates that *d6r* units in solution do not promote the nucleation of AFI', we find epitaxy between the flat 6-member rings of CHA and the puckered ones of AFI' (Figure 5b).

CHA is a member of the ABC-6 family,[52-54] the crystals of which are built by stacking of a monolayer that has domain matching with the (001) planes of AFI and AFI' (Figure 5e-g). The simulations demonstrate that the binding between the zeolites takes advantage of the domain matching between CHA and AFI' planes, with AFI' 12-member ring channels aligning with the basal plane of the *d6r* rings, as depicted in Section E of the SI. The domain matching is enabled by their identical spacing and order of the 12-member rings of CHA and AFI'. We anticipate the same for CHA and AFI whereby we conjecture that the similarities between the CHA and AFI (001) planes (Figure 5f-g) favor the formation of an ITL that decreases the energetic cost of the zeolite/zeolite interface and facilitates their cross-nucleation.

2.5. CHA can promote the nucleation of AFI' from dilute solutions of reactants.

Zeolite growth mixtures comprise a diverse range of silicate species in the solid and solution states that can participate in crystallization. The high concentration of silica at the onset of syntheses leads to the formation of amorphous precursor nanoparticles, which can dynamically exchange species with those in solution; however, as the amorphous precursors are consumed, crystal growth at later stages of the synthesis tends to be dominated by the addition of small oligomers and monomeric silica species present in solution. Here we investigate whether small oligomers and monomers attaching to the CHA seed from a dilute solution result in the cross nucleation and growth of the daughter zeolite.

To investigate whether the CHA (001) surface can promote the nucleation of AFI' in dilute (i.e., low supersaturation) silica growth environments, we proceed as in Section 2.2, inserting OSDA and silica monomers in a ratio 1:12 into a simulation cell in which CHA exposes the (001) face to the implicit solvent solution. The rate of appearance of the reactants in the simulation cell is selected to be slow enough to prevent the formation of large amorphous aggregates in the solution (see Methods 4.2); however, this rate still results in the sporadic

formation of oligomers with up to ~6 silica units and, very rarely, the formation of small amorphous clusters that contain up to ~40 silica units before reaching the CHA surface. Figure 6 and Movies 4 and 5 depict the temporal evolution along the low-supersaturation simulation. We find that, irrespective of their size, the oligomers and clusters reorder at the interface, losing memory of their original configuration.

The cross-nucleation of AFI' on CHA from solution shares most characteristics with the cross-nucleation from the amorphous phase. First, the ITL ordering precedes AFI' cross nucleation from solution (compare Figure 4 and Figure S5). Second, AFI' cross-nucleates at the CHA interface, with AFI' cross-nucleating perpendicular to the CHA surface. Third, the AFI' is bound to the CHA (001) face via the same interfacial transition layer (ITL) described in Section 2.4. We conclude that the mechanism of cross-nucleation is robust to large changes in silica concentration.

The formation of AFI' on CHA from solution is limited by the access of silica and OSDA to the seed, which we control by the insertion rate of the reactants into the simulation cell. We take advantage of the slower crystallization from solution to follow the details of the molecular mechanisms that lead to IZT through cross-nucleation (Figure 6). The first deposited silica particles quickly organize into *d6r*-like cages upon adsorption to the CHA (001) interface (Figure 6a). These initial *d6r* cages are transient and appear across the surface (red motifs in Figure 6a). The OSDAs diffuse across the CHA/solution interface, preferentially adsorbing onto the exposed *d6r* of CHA. As the system evolves, the newly formed *d6r* cages reorganize into ITL patches, surrounding and eventually sequestering the OSDAs (Movie 6). An OSDA adsorbed to a specific location on the CHA surface prevents silica from attaching there, and vice versa. This dynamic interaction between silica and OSDA shapes the structure of the interface. Notably, the silica at the CHA (001) interface adopts two competing interfacial orders (Figure 6b and 6c). AFI' emerges from the ITL order described in Section 2.4 (~5 nm diameter circled regions in Figure 6b-c). The results presented in Figure 6, together with the lack of ability of CHA CBUs to promote the formation of AFI, suggest that a minimum ITL size is required to establish the domain matching necessary for heterogeneous AFI' nucleation at the CHA interface.

After the successful nucleation of AFI' on the ITL patch, the 1D pore zeolite grows along the CHA interface, resulting in the concurrent transformation of the non-nucleating interfacial order into the one of the ITL that connects AFI' to CHA (Movie 5). Crystallization of AFI' progresses first to cover all the CHA surface in the simulation cell, and then proceeds to grow layer-by-layer with its 1D pores oriented normal to the seed interface. The complete wetting of the CHA surface by AFI' is consistent with the strong binding free energy between these zeolites. We conclude that the CHA (001) surface strongly promotes the nucleation and growth of the 1D zeolite even with highly diluted reactants, consistent with experimental observations.[4]

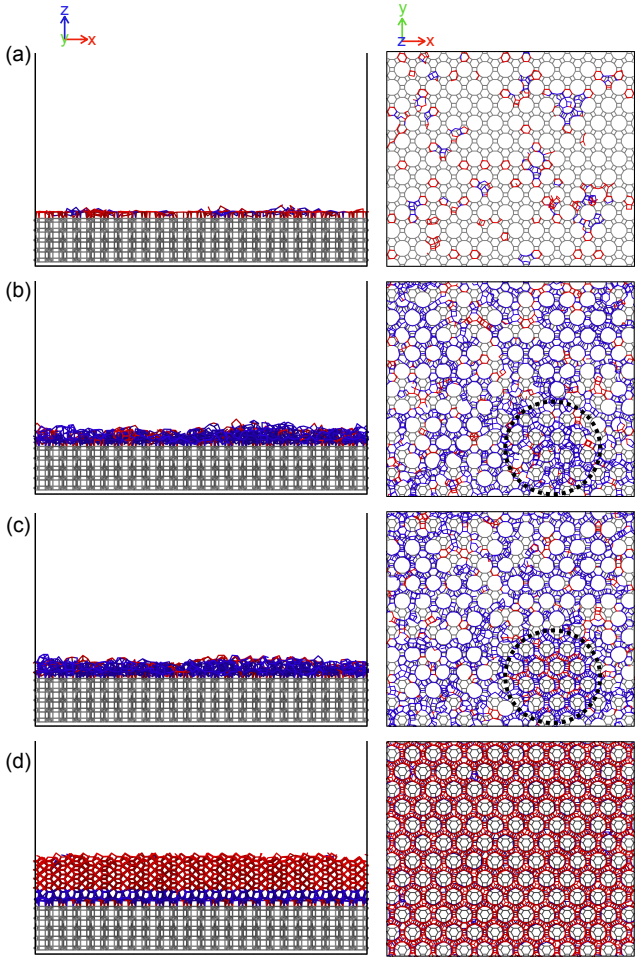

Figure 6. Cross-nucleation from solution of AFI' on the (001) face of zeolite CHA. Snapshots (a)-(d) represent different points in time along the evolution of the system. Left and right panels show side views and top views of the simulation cell, respectively. In this case, silica and OSDA particles are deposited at a rate of one particle every 30 ps and 360 ps, respectively. Only bonds between silica are shown; OSDAs are omitted for clarity. The coloring scheme is as follows. The CHA slab is shown in gray. Deposited silicate species are colored according to their crystallinity as characterized by the order parameter: red is crystalline and blue is amorphous. Note that the order parameter identifies elements such as *d6r*, which do not constitute AFI', as crystalline. The right side panels show only the surface layer of CHA so that the alignment of the ITL and AFI' are easier to identify. The dashed circles on the right-side panels of (b) and (c) enclose the origin of the ITL ordering, where AFI' nucleation occurs.

3. CONCLUSIONS

In this study we use molecular simulations and nucleation theory to address the critical, albeit understudied, question of how a parent zeolite can accelerate or direct the formation of another zeolite polymorph. We focus on the challenging case in which the parent seed crystal does not share a common plane or CBU with the daughter. Inspired by the report of acceleration of the synthesis of AFI by CHA seeds, we investigate the nucleation of AFI' -a proxy for AFI- in the absence of seeds, as well as in the presence CHA and its CBUs. To our knowledge, this is the first study to investigate zeolite seeding mechanisms using molecular simulations.

The predominant paradigm for seed-assisted zeolite synthesis proposes that the seed zeolite induces an interzeolite transformation by dissolving into structural units (SBUs or CBUs), which assist in the nucleation of the daughter crystal. Our simulations indicate that CBUs of CHA dispersed in solution or in the amorphous precursor mixture do not facilitate the nucleation of the AFI' zeolite. Our study does not exclude the possibility that parent/daughter pairs with common CBUs might use these units as seeds for the nucleation and/or growth of the daughter phase, provided that those CBUs exist in solution and have a sufficiently long lifetime. However, experimental studies to date do not support these pre-conditions.[13-14]

Crucially, our simulations demonstrate that cross-nucleation of the daughter zeolite on the parent seed is a feasible pathway for interzeolite transformation in seed-assisted synthesis, as even pairs of zeolites lacking a common plane or CBU can undergo cross-nucleation if they exhibit domain matching on some crystal plane. Epitaxy through domain matching has been proposed for other pairs of zeolites, such as UTD-1/AFI[14] and CHA/DDR[53], but never demonstrated at the molecular level. Our simulations show that domain matching assists in the formation of a stable interfacial transition layer between parent and daughter, lowering the barrier for cross-nucleation. In the absence of domain matching between the parent and daughter zeolites, we expect that the effects of distortions would accumulate along extended distances, destabilizing the interface between them. A less stable ITL would have diminished efficiency for cross-nucleation, although it may still enable epitaxy between the crystals.[55]

Supersaturation levels fluctuate throughout the synthesis, decreasing as reactants are utilized. We find that the ability of CHA to nucleate AFI' is robust to changes of the silica to OSDA ratios and water content in the synthesis mixtures, consistent with the finding of robust enhancement of AFI formation in the presence of CHA in experiments with a wide range of experimental conditions.[4]

Classical nucleation theory indicates that the nucleation barrier increases with the energetic cost of generating a seed-daughter interface.[19-20] Seeds that closely match the nucleating crystal, reduce structural distortions, minimizing the energy cost of the interface. The corollary is that if zeolites without common planes can cross-nucleate, as we show in the present study, then zeolite pairs with common planes could do so even more readily. Based on our results and analyses, we propose that the most promising candidates for cross-nucleation are pairs of zeolites that form intergrowths, as these polymorphs share a common crystal plane and, thus, would not necessitate the formation of a distinct interfacial transition layer to connect the two zeolite polymorphs. This is a likely case for the synthesis of MOR and MFI from MEL seeds,[56] as both MOR/MFI [57] and MFI/MEL[58] form intergrowths. Interestingly, MEL seeds can promote the formation of MFI at conditions where homogeneous synthesis produces MOR.[23, 56] That result, together with the ability of CHA to promote AFI at conditions that result in a layered silicate in the absence of the seed,[4] support that cross-nucleation can result in structural selectivity by lowering the barriers for the formation of specific zeolites.

4. SIMULATION METHODS

4.1. Model. We model the zeolite nucleation and growth using a many-body coarse-grained reactive (CG-Rx) model[43] that comprises two distinct types of particles: a silica particle T, and an organic structure directing agent particle S. The water solvent and mineralizers are treated implicitly by encoding their influence in the interactions between the T and S particles. Importantly, this model circumvents much of the chemistry involved in reforming the silica network —i.e. hydrolysis and condensation—relying, rather, on simple interactions to represent silica-silica bonding. The simplicity of the model, both in terms of the number of components and complexity of interactions, makes it several orders of magnitude computationally more efficient than all-atom models.

The silica-silica interactions in the CG-Rx model are a sum of two- and three-body interactions with the TS-λ=4 parameterization.[43] The two-body interaction is a parameterization of the two-body the Stillinger-Weber[59] potential (SW), and the three-body term is parameterized to mimic the broader range of Si-Si-Si angles in zeolites.[43] The parameters for the three-body T-T-T term can be obtained from ref. 43 or downloaded from GitHub.[60]

The S-S and T-S particles interact solely through the two-body term of SW with parameters that stabilize the twelve-member ring in AFI (Table 1). The other parameters of the two-body SW potential are the same as in ref. 59: = 7.049556277, $B = 0.602224558$, $p = 4$, $q = 0$, $a = 1.8$, and $\gamma = 1.2$ for all interactions.

Table 1. Energy and size scale parameters for the two-body interaction between silica (T) and the OSDA (S) in the model.

Interaction	ε (kcal/mol)	σ (Å)
T–T	12.378	2.7275
S–S	0.68	7.0
T–S	1.6	6.0

SSZ-24, the pure silica AFI framework, has one $TMAda^+$ per unit cell.[48, 61] We represent the volume of a single $TMAda^+$ with 2 S molecules, which we add to a unit cell of AFI (downloaded from the International Zeolite Association structure database[62]). AFI minimized with the coarse-grained model restructures to AFI', which has 12-member ring 1D channel structures and other features similar to AFI (see Section 2.4 and SI Section C). The melting temperature of AFI' (determined by following the procedures of refs 37, 43) is 835 ± 1 K for the T:S ratio 9:1, 871 ± 1 K for the T:S ratio 12:1 (SI Section F), and 870 ± 1 K for the T:S ratio 16:1.

4.2. Simulation settings. Molecular dynamics simulations are run using LAMMPS.[63] The velocity Verlet algorithm is used to integrate the equations of motion with a time step of 5 fs. Periodic boundary conditions are set in the three Cartesian directions. The in the isobaric-isothermal (*NpT*) ensemble use the Nose-Hoover thermostat and barostat with damping times of 1 and 5 ps, respectively, with the pressure set to 1 atm and the temperature to 620 K, except for the cooling ramps in which it is decreased linearly at a rate of 1 Kns^{-1}. Simulations in the canonical (*NVT*) ensemble use the Nose-Hoover thermostat with a damping constant of 1 ps when the system involves a dense amorphous precursor phase, or the Langevin thermostat with a friction coefficient of 1 ps^{-1} when the precursor is a dilute solution. Each simulation is run for hundreds of nanoseconds to ensure the nucleation and growth of the AFI' zeolite. The simulations presented in this work amount to a total evolution of ~39 microseconds.

4.3. Simulation systems. Using LAMMPS, we randomly generate dense amorphous precursor phases with silica to OSDA ratios 12:1 and 8:1 and a total of 11232 T and S particles. These mixtures are pre-equilibrated at 630 K for 100 ns and subsequently at 620 K for 0.5 ns. Multiple initial amorphous configurations are obtained by evolving the system for an additional 5 ns at 620 K, retrieving configurations every 0.5 ns (sufficiently far apart to avoid artifacts due to correlations). We verify that none of these initial simulations contained AFI'.

The seedless, homogeneous nucleation simulations start with the pre-equilibrated amorphous phases described above. We evolve 49 independent simulations in the absence of the seed for up to 600 ns using system A1 of Table S5. The top 4 nm of the box are occupied by a vacuum layer to accommodate the change in volume as the amorphous phase crystallizes to AFI'. All of these trajectories exhibit homogeneous nucleation of AFI', which we detect by both the sudden decrease in the potential energy of the simulation cell and the appearance of crystallites recognized with our order parameters (see Section 4.4). The homogeneous nucleation is characterized by long nucleation times and random orientation of the resulting AFI' crystal within the simulation cell. We also prepared a simulation cell, system A11 with a dense amorphous precursor with T:S ratio 8:1, which we pre-equilibrate at 800 K and 1 atm for 2.5 ns, then evolved for 100 ns at 620 K (no crystallization is observed), and finally cooled to 450 K at a rate of 1 K/ns to record the temperature at which there is crystallization. The results of all seedless simulations are discussed in Section 2.1.

To test whether a single CHA CBU can promote the formation of AFI' from a dilute solution of the reactants, we position a *cha* ($4^{12}6^2 8^6$) cage at the center of a cubic simulation box using system D1 of Table S5; the corresponding results are shown in Section 2.2. The equations of motion for the *cha* cage are not integrated, i.e. it is considered a fixed rigid body, to avoid its dissolution. To model the seeding under dilute conditions, we assume that low amounts of silica and OSDA diffuse in the solution to meet the CBU. To this intend, T and S particles are randomly generated outside a spherical region with a 15 Å radius centered around the *cha* cage. To maintain a constant T:S ratio (12:1) throughout the simulation, the rate of insertion of S is twelve times the rate of one T particle every 50 ps. The insertion proceeds over 150 ns. The resulting amorphous particle has a ~7 nm diameter, consistent with the typical size of amorphous precursors in zeolite synthesis.[50-51] The system is then allowed to evolve without any further addition of T or S for 390 ns.

Simulations of nucleation in the presence of CHA's CBUs and a pre-equilibrated amorphous precursor phase are performed using systems A5-A10 of Table S5. The top 4 nm of the box is occupied by a vacuum layer to accommodate the change in volume as the amorphous phase crystallizes to AFI'. The rigid CBUs are inserted randomly into the simulation cell, and a small cubic volume of amorphous particles is removed at each insertion point to prevent unfavorable interactions due to particle overlap. Table S3 presents the total number of independent simulations and the number and type of CBUs in each. The CBUs are treated as rigid but able to diffuse within the precursor phase. These systems evolve for up to 600 ns or

until crystallization is observed. The corresponding results are discussed in Section 2.2.

To create the CHA slab for the seeded simulations, we obtain the crystal CIF file from the zeolite database [62]. We remove the oxygen atoms and keep the Si atoms as the locus of the T particles. We add 2 S molecules into each cha cage of CHA and transform the triclinic unit cell into an orthogonal cell. This simple transformation is done by replicating the triclinic unit cell in the *x*-axis and *y*-axis by two and subsequently using periodic boundary conditions to map the particles into an orthorhombic cell. This final cell contains 24 S and 144 T particles. To create the seed in our study, the orthogonal CHA cell is replicated 3 times in *x* and *y* and 2 times in *z*. This results in a slab of CHA that, in the cross-nucleation simulations, is held rigid by not integrating the equations of motion of its T particles, while the OSDAs within the CHA framework are allowed to move. The CHA slab exposes the (001) crystal face and contains 2160 T particles and 288 S particles. It is important to note that the bottom of the slab does not interact with the amorphous precursor because it is buffered by a slab of vacuum which enables the expansion of the amorphous mixture as it crystallizes into AFI'.

To investigate the nucleation of AFI' from the dense amorphous precursors in the presence of CHA, we perform simulations with the systems A2, A3 and A4 of Table S5. The top 4 nm of the box is occupied by a vacuum layer to accommodate the change in volume as the amorphous phase crystallizes to AFI'. In the simulation starting with system A2, the dense amorphous precursor phase is pre-equilibrated in contact with CHA at 630 K for 5 ns and then set to 620 K. Simulations with the systems A3 and A4 are arranged so that the (001) face of the CHA slab is initially separated from the pre-equilibrated amorphous phase by a narrow gap in *z* of about 1 nm. This setup is used to model the encounter of a pre-equilibrated amorphous precursor particle with the CHA seed. The difference between A3 and A4 is the size of the simulation cell. In A4 we double the *x* and *y* dimensions of the cells, making a 4 times larger area of CHA, and remove the half the amorphous phase farther from the CHA surface, concomitantly decreasing the height (*z*-direction) of the box. Figures 4 and S5 show snapshots of this wider simulation cell. We run 19 independent simulations of nucleation with system A2, 13 with system A3, and 2 with system A4. We evolve these 34 simulations for 20 ns, resulting in the crystallization of AFI' in 31 of them. These results are discussed in Sections 2.3 and 2.4.

To examine the impact of altering the composition of the amorphous mixture on the formation of AFI' from the dense amorphous mixture in the presence of CHA, we use system A12 in which the T:S ratio of the amorphous mixtures in systems A2 is altered in LAMMPS to 8:1. The amorphous precursor in contact with CHA is first equilibrated at 800 K for 2.5 ns, followed by 100 ns at 620 K. As the system does not crystallize, we cool it from 620 K to 550 K at a rate of 1K/ns to record the crystallization temperature and compare with the one of homogeneous nucleation for the same composition and cooling rate. The comparison of the homogeneous and heterogeneous nucleation with 8:1 composition of is presented in Section 2.3 and Table S4.

To investigate the nucleation of AFI' from a dilute solution in the presence of CHA, we a simulation cell that exposes the (001) plane of CHA to an initially empty environment where T and S particles are inserted up to the numbers shown in system D2 of Table S5. A repulsive wall at the end along the z-direction ensures particles deposit only on one side of the slab. To maintain a constant 12:1 T:S ratio throughout the simulation, the rate of insertion of S is twelve times that of T. The particle deposition rate (1 T particle every 30 ps) ensures that particles attach to the CHA slab as monomers or small oligomers rather than forming larger amorphous precursor clusters in solution before reaching the CHA surface. This simulation is run over 70 ns with constant deposition rates through the entire trajectory, over which we detect the formation of the ITL and AFI'.

4.4. Zeolite identification. We identify T particles that belong to the AFI' or CHA zeolite crystals by the use of the averaged form of the local bond order parameter $\bar{q}_l$ [64] with spherical harmonics of order $l = 8$:

$$\bar{q}_l(i) = \sqrt{\frac{4\pi}{2l+1}\sum_{m=-l}^{l}|\bar{q}_{lm}(i)|^2}, \quad (1)$$

where

$$\bar{q}_{lm}(i) = \frac{1}{\tilde{N}_b(i)}\sum_{k=0}^{\tilde{N}_b} q_{lm}(k), \quad (2)$$

and $\tilde{N}_b$ accounts for all neighbors of particle i plus the particle i itself. The complex vector q_{lm} is defined as:

$$q_{lm}(k) = \frac{1}{N_b(k)}\sum_{j=1}^{N_b} Y_{lm}(r_{kj}), \quad (3)$$

where $N_b(k)$ is the number of neighbors of particle k. $Y_{lm}(r_{kj})$ are the spherical harmonics functions and r_{kj} is the vector from particle k to particle j. We consider neighbor particles to be within a cutoff of 5 Å (the distance of nearest T neighbors). Figure 7 shows that the ordering of the T particles is zeolitic when $\bar{q}_8 > 0.3$. This order parameter selects for both AFI' and CHA ordering, because the distribution of $\bar{q}_8$ corresponding to CHA overlaps with that of AFI', and therefore, cannot be used to discriminate between the two crystals (which are easily distinguished by size and connectivity of the pores). Moreover, $\bar{q}_8$ does not discern the ordering of the interfacial transition layer, classifying it as amorphous or non-zeolitic.

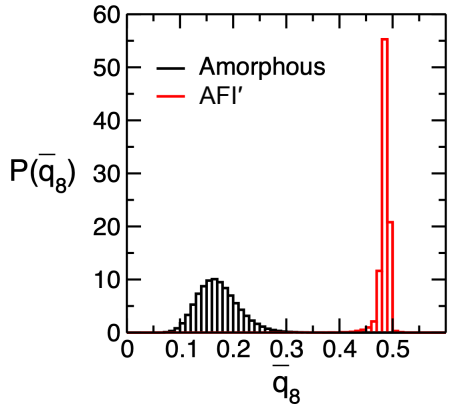

Figure 7. The histogram of $\bar{q}_8$ values computed for T particles in the amorphous phase (black) and AFI' crystal (red) show that these two phases are well differentiated with our order parameter.

Corresponding Author's email: valeria.molinero@utah.edu

Supporting Information.

The Supporting Information file includes: a discussion of the effect of synthesis conditions on AFI crystallization (Section A), a comparison of homogeneous and heterogeneous nucleation (Section B), a detailed analysis of the AFI' framework structure (Section C), an explanation of the methods used to determine the orientation of AFI' pores and the resulting distribution of these orientations (Section D), a description of the stages involved in ITL ordering along with a comprehensive overview of its structure (Section E), a summary of simulations exploring AFI' nucleation in the presence of CHA CBUs and an overview of all simulations conducted (Section F), and descriptions of supplementary movies (Section G).

Funding. This work was supported by the United States Department of Energy through BES Condensed Phase and Interfacial Molecular Science (CPIMS) program through award DE-SC0023213.

Acknowledgements. We the Center of High Performance Computing at The University of Utah for technical support and a grant of computer time.

References.

(1) Jain, R.; Mallette, A. J.; Rimer, J. D. Controlling Nucleation Pathways in Zeolite Crystallization: Seeding Conceptual Methodologies for Advanced Materials Design. *J Am Chem Soc* **2021,** *143*, 21446-21460.

(2) Devos, J.; Shah, M. A.; Dusselier, M. On the Key Role of Aluminium and Other Heteroatoms during Interzeolite Conversion Synthesis. *RSC advances* **2021,** *11*, 26188-26210.

(3) Mallette, A. J.; Shilpa, K.; Rimer, J. D. The Current Understanding of Mechanistic Pathways in Zeolite Crystallization. *Chem Rev* **2024,** *124*, 3416-3493.

(4) Tang, L.; Haw, K.-G.; He, P.; Fang, Q.; Qiu, S.; Valtchev, V. Synthesis of Zeolite Ssz-24 Using a Catalytic Amount of Ssz-13 Seeds. *Inorganic Chemistry Frontiers* **2019,** *6*, 3097-3103.

(5) Hou, L.-Y.; Thompson, R. W. Stability and Growth of Silicalite Seeds: An Observation of Initial Breeding. *Zeolites* **1989,** *9*, 526-530.

(6) Goel, S.; Zones, S. I.; Iglesia, E. Synthesis of Zeolites Via Interzeolite Transformations without Organic Structure-Directing Agents. *Chem Mater* **2015,** *27*, 2056-2066.

(7) Keiji, I.; Yoshihiro, K.; Kenta, I.; Atsushi, S.; Tatsuya, O. A Working Hypothesis for Broadening Framework Types of Zeolites in Seed-Assisted Synthesis without Organic Structure-Directing Agent. *J. Am. Chem. Soc.* **2012,** *134*, 11542-11549.

(8) Wang, Y.; Li, X.; Xue, Z.; Dai, L.; Xie, S.; Li, Q. Preparation of Zeolite Ana Crystal from Zeolite Y by in Situ Solid Phase Iso-Structure Transformation. *J Phys Chem B* **2010,** *114*, 5747-5754.

(9) Goto, I.; Itakura, M.; Shibata, S.; Honda, K.; Ide, Y.; Sadakane, M.; Sano, T. Transformation of Lev-Type Zeolite into Less Dense Cha-Type Zeolite. *Micropor Mesopor Mat* **2012,** *158*, 117-122.

(10) Li, C.; Moliner, M.; Corma, A. Building Zeolites from Precrystallized Units: Nanoscale Architecture. *Angewandte Chemie International Edition* **2018,** *57*, 15330-15353.

(11) Suhendar, D.; Buchari; Mukti, R.; Ismunandar In *Simple Approach in Understanding Interzeolite Transformations Using Ring Building Units*, IOP Conference Series: Materials Science and Engineering, IOP Publishing: 2018; p 012016.

(12) Jon, H.; Ikawa, N.; Oumi, Y.; Sano, T. An Insight into the Process Involved in Hydrothermal Conversion of Fau to* Bea Zeolite. *Chem Mater* **2008,** *20*, 4135-4141.

(13) Pelster, S. A.; Kalamajka, R.; Schrader, W.; Schüth, F. Monitoring the Nucleation of Zeolites by Mass Spectrometry. *Angewandte Chemie International Edition* **2007,** *46*, 2299-2302.

(14) Pelster S. A.; Weimann, B.; Schaack, B. B.; Schrader, W.; Schüth, F. Dynamics of silicate species in solution studied by

mass spectrometry with isotopically labeled compounds. *Angewandte Chemie International Edition* **2007,** *46*, 6674-7.
(15) Cundy, C. S.; Cox, P. A. The Hydrothermal Synthesis of Zeolites: Precursors, Intermediates and Reaction Mechanism. *Micropor Mesopor Mat* **2005,** *82*, 1-78.
(16) Valtchev, V.; Paillaud, J. L.; Kessler, H.; Creyghton, E. J. Inductive Effect of Template Containing Utd-1 Seeds on the Synthesis of Zeolite Ssz-24. *Micropor Mesopor Mat* **1999,** *33*, 143-148.
(17) Nguyen, A. H.; Molinero, V. Cross-Nucleation between Clathrate Hydrate Polymorphs: Assessing the Role of Stability, Growth Rate, and Structure Matching. *J Chem Phys* **2014,** *140*, 084506.
(18) Nguyen, A. H.; Jacobson, L. C.; Molinero, V. Structure of the Clathrate/Solution Interface and Mechanism of Cross-Nucleation of Clathrate Hydrates. *J Phys Chem C* **2012,** *116*, 19828-19838.
(19) Qiu, Y.; Odendahl, N.; Hudait, A.; Mason, R.; Bertram, A. K.; Paesani, F.; DeMott, P. J.; Molinero, V. Ice Nucleation Efficiency of Hydroxylated Organic Surfaces Is Controlled by Their Structural Fluctuations and Mismatch to Ice. *J Am Chem Soc* **2017,** *139*, 3052-3064.
(20) Turnbull, D. Kinetics of Heterogeneous Nucleation. *J Chem Phys* **1950,** *18*, 198-203.
(21) Wang, Y.; Tong, C.; Liu, Q.; Han, R.; Liu, C. Intergrowth Zeolites, Synthesis, Characterization, and Catalysis. *Chem Rev* **2023,** *123*, 11664-11721.
(22) Schwalbe-Koda, D.; Jensen, Z.; Olivetti, E.; Gómez-Bombarelli, R. Graph Similarity Drives Zeolite Diffusionless Transformations and Intergrowth. *Nat Mater* **2019,** *18*, 1177-1181.
(23) Chawla, A.; Mallette, A. J.; Jain, R.; Le, N.; Hernández, F. C. R.; Rimer, J. D. Crystallization of Potassium-Zeolites in Organic-Free Media. *Micropor Mesopor Mat* **2022,** *341*, 112026.
(24) Grand, J.; Awala, H.; Mintova, S. Mechanism of Zeolites Crystal Growth: New Findings and Open Questions. *Crystengcomm* **2016,** *18*, 650-664.
(25) Hong, S.; Mallette, A. J.; Neeway, J. J.; Motkuri, R. K.; Rimer, J. D.; Mpourmpakis, G. Understanding Formation Thermodynamics of Structurally Diverse Zeolite Oligomers with First Principles Calculations. *Dalton Transactions* **2023,** *52*, 1301-1315.
(26) Yang, C.-S.; Mora-Fonz, J. M.; Catlow, C. R. A. Stability and Structures of Aluminosilicate Clusters. *J Phys Chem C* **2011,** *115*, 24102-24114.
(27) Yang, C.-S.; Mora-Fonz, J. M.; Catlow, C. R. A. Modeling the Polymerization of Aluminosilicate Clusters. *J Phys Chem C* **2012,** *116*, 22121-22128.
(28) Yang, C.-S.; Mora-Fonz, J. M.; Catlow, C. R. A. Modeling the Nucleation of Zeolite A. *J Phys Chem C* **2013,** *117*, 24796-24803.
(29) White, C. E.; Provis, J. L.; Kearley, G. J.; Riley, D. P.; Van Deventer, J. S. Density Functional Modelling of Silicate and Aluminosilicate Dimerisation Solution Chemistry. *Dalton transactions* **2011,** *40*, 1348-1355.
(30) Freeman, E. E.; Neeway, J. J.; Motkuri, R. K.; Rimer, J. D.; Mpourmpakis, G. Understanding Initial Zeolite Oligomerization Steps with First Principles Calculations. *AIChE Journal* **2020,** *66*, e17107.
(31) Pereira, J.; Catlow, C.; Price, G. Silica Condensation Reaction: An Ab Initio Study. *Chemical Communications* **1998**, 1387-1388.
(32) Mora‐Fonz, M. J.; Catlow, C. R. A.; Lewis, D. W. Oligomerization and Cyclization Processes in the Nucleation of Microporous Silicas. *Angewandte Chemie* **2005,** *117*, 3142-3146.
(33) Mora-Fonz, M. J.; Catlow, C. R. A.; Lewis, D. W. Modeling Aqueous Silica Chemistry in Alkali Media. *J Phys Chem C* **2007,** *111*, 18155-18158.
(34) Mora-Fonz, M. J.; Catlow, C. R. A.; Lewis, D. W. H-Bond Interactions between Silicates and Water during Zeolite Pre-Nucleation. *Physical Chemistry Chemical Physics* **2008,** *10*, 6571-6578.
(35) Van Duin, A. C.; Dasgupta, S.; Lorant, F.; Goddard, W. A. Reaxff: A Reactive Force Field for Hydrocarbons. *The Journal of Physical Chemistry A* **2001,** *105*, 9396-9409.
(36) Jing, Z.; Xin, L.; Sun, H. Replica Exchange Reactive Molecular Dynamics Simulations of Initial Reactions in Zeolite Synthesis. *Physical Chemistry Chemical Physics* **2015,** *17*, 25421-25428.
(37) Dhabal, D.; Bertolazzo, A. A.; Molinero, V. Coarse-Grained Model for the Hydrothermal Synthesis of Zeolites. *J Phys Chem C* **2021,** *125*, 26857-26868.
(38) Kumar, A.; Zare, M.; Molinero, V. Assembly of Zeolitic Crystals from a Model of Mesogenic Patchy Nanoparticles. *J Phys Chem C* **2019,** *123*, 971-978.
(39) Kumar, A.; Nguyen, A. H.; Okumu, R.; Shepherd, T. D.; Molinero, V. Could Mesophases Play a Role in the Nucleation and Polymorph Selection of Zeolites? *J Am Chem Soc* **2018,** *140*, 16071-16086.
(40) Jin, L.; Auerbach, S. M.; Monson, P. A. Emergence of Zeolite Analogs and Other Microporous Crystals in an Atomic Lattice Model of Silica and Related Materials. *J Phys Chem Lett* **2012,** *3*, 761-765.
(41) Chien, S.-C.; Auerbach, S. M.; Monson, P. A. Reactive Ensemble Monte Carlo Simulations of Silica Polymerization That Yield Zeolites and Related Crystalline Microporous Structures. *J Phys Chem C* **2015,** *119*, 26628-26635.
(42) Bores, C.; Luo, S.; David Lonergan, J.; Richardson, E.; Engstrom, A.; Fan, W.; Auerbach, S. M. Monte Carlo Simulations and Experiments of All-Silica Zeolite Lta Assembly Combining Structure Directing Agents That Match Cage Sizes. *Physical Chemistry Chemical Physics* **2022,** *24*, 142-148.
(43) Bertolazzo, A. A.; Dhabal, D.; Lopes, L. J. S.; Walker, S. K.; Molinero, V. Unstable and Metastable Mesophases Can Assist in

the Nucleation of Porous Crystals. *J Phys Chem C* **2022,** *126*, 3776-3786.
(44) Bores, C.; Auerbach, S. M.; Monson, P. A. Enhanced Replica Exchange Reactive Monte Carlo Simulations for Constructing Zeolite Frameworks. *Molecular Simulation* **2018,** *44*, 453-462.
(45) Dhabal, D.; Bertolazzo, A. A.; Molinero, V. What Is the Smallest Zeolite That Could Be Synthesized? *Angew. Chem. Int. Ed.* **2022,** *61*, e202205095.
(46) Bertolazzo, A. A.; Dhabal, D.; Molinero, V. Polymorph Selection in Zeolite Synthesis Occurs after Nucleation. *J Phys Chem Lett* **2022,** *13*, 977-981.
(47) Kumar, A.; Molinero, V. Two-Step to One-Step Nucleation of a Zeolite through a Metastable Gyroid Mesophase. *J Phys Chem Lett* **2018,** *9*, 5692-5697.
(48) Gittleman, C. S.; Watanabe, K.; Bell, A. T.; Radke, C. J. A Mechanistic Study of the Synthesis of Zeolite Ssz-24. *Microporous Materials* **1996,** *6*, 131-150.
(49) Liu, Z.; Zhu, J.; Wakihara, T.; Okubo, T. Ultrafast Synthesis of Zeolites: Breakthrough, Progress and Perspective. *Inorganic Chemistry Frontiers* **2019,** *6*, 14-31.
(50) Mintova, S.; Olson, N. H.; Senker, J.; Bein, T. Mechanism of the Transformation of Silica Precursor Solutions into Si ‐ Mfi Zeolite. *Angewandte Chemie* **2002,** *114*, 2670-2673.
(51) Fedeyko, J. M.; Rimer, J. D.; Lobo, R. F.; Vlachos, D. G. Spontaneous Formation of Silica Nanoparticles in Basic Solutions of Small Tetraalkylammonium Cations. *J Phys Chem B* **2004,** *108*, 12271-12275.
(52) Millward, G.; Ramdas, S.; Thomas, J. M. On the Direct Imaging of Offretite, Cancrinite, Chabazite and Other Related Abc-6 Zeolites and Their Intergrowths. *Proceedings of the Royal Society of London. A. Mathematical and Physical Sciences* **1985,** *399*, 57-71.
(53) Akporiaye, D. E. Structural Relations of Zeolite Frameworks: Abc-6 and Other Frameworks Derived from Hexagonal 4.6.12 and (4.6.8)1(4.8.12)1 3-Connected Nets. *Zeolites* **1992,** *12*, 197-201.
(54) Baerlocher, C.; McCusker, L. B. The ABC-6 Family in https://america.iza-structure.org/IZA-SC/DO_structures/DO_family_table.html. Accessed on February 1 2024.
(55) Factorovich, M. H.; Naullage, P. M.; Molinero, V. Can Clathrates Heterogeneously Nucleate Ice? *J Chem Phys* **2019,** *151*, 114707.
(56) Jain, R.; Rimer, J. D. Seed-Assisted Zeolite Synthesis: The Impact of Seeding Conditions and Interzeolite Transformations on Crystal Structure and Morphology. *Micropor Mesopor Mat* **2020,** *300*, 110174.
(57) Hong, Z.; Li, J.; Xiong, C.; Zhao, G.; Wang, X.; Zhu, Z. Creation of Cross Directing Intergrowth Mor/Zsm-5 with High Catalytic Activity: Insights into the Role of Crystallization Time. *Micropor Mesopor Mat* **2021,** *320*, 111102.
(58) Alberti, A.; Vezzalini, G. The Thermal Behaviour of Heulandites: A Structural Study of the Dehydration of Nadap Heulandite. *Tscher. Mineral. Petr. Mitt.* **1983,** *31*, 259-270.
(59) Stillinger, F. H.; Weber, T. A. Computer Simulation of Local Order in Condensed Phases of Silicon. *Physical Review B* **1985,** *31*, 5262-5271.
(60) Lopes, L. J. S. https://github.com/laurajoanalopes/swpoly.
(61) Van Nordstrand, R. A.; Santilli, D. S.; Zones, S. I., An All-Silica Molecular Sieve That Is Isostructural with Alpo4-5. In *Perspectives in Molecular Sieve Science*, American Chemical Society: 1988; Vol. 368, pp 236-245.
(62) Baerlocher, C.; McCusker, L. B. Database of Zeolite Structures. http://www.iza-structure.org/databases/. Accessed on February 1 2024.
(63) Thompson, A. P.; Aktulga, H. M.; Berger, R.; Bolintineanu, D. S.; Brown, W. M.; Crozier, P. S.; in't Veld, P. J.; Kohlmeyer, A.; Moore, S. G.; Nguyen, T. D. Lammps-a Flexible Simulation Tool for Particle-Based Materials Modeling at the Atomic, Meso, and Continuum Scales. *Computer Physics Communications* **2022,** *271*, 108171.
(64) Lechner, W.; Dellago, C. Accurate Determination of Crystal Structures Based on Averaged Local Bond Order Parameters. *J Chem Phys* **2008,** *129*, 114707.

Table of Contents Figure